



HAL
open science

Oxidative Sequence of a Ruthenocene-Based Anticancer Drug Candidate in a Basic Environment

Hui Zhi Shirley Lee, Olivier Buriez, Eric Labbé, Siden Top, Pascal Pigeon, Gérard Jaouen, Christian Amatore, Weng Kee Leong

► **To cite this version:**

Hui Zhi Shirley Lee, Olivier Buriez, Eric Labbé, Siden Top, Pascal Pigeon, et al.. Oxidative Sequence of a Ruthenocene-Based Anticancer Drug Candidate in a Basic Environment. *Organometallics*, 2014, 33 (18), pp.4940-4946. 10.1021/om500225k . hal-01230374

HAL Id: hal-01230374

<https://hal.science/hal-01230374>

Submitted on 5 Apr 2024

HAL is a multi-disciplinary open access archive for the deposit and dissemination of scientific research documents, whether they are published or not. The documents may come from teaching and research institutions in France or abroad, or from public or private research centers.

L'archive ouverte pluridisciplinaire **HAL**, est destinée au dépôt et à la diffusion de documents scientifiques de niveau recherche, publiés ou non, émanant des établissements d'enseignement et de recherche français ou étrangers, des laboratoires publics ou privés.

Oxidative Sequence of a Ruthenocene-Based Anticancer Drug Candidate in a Basic Environment

Hui Zhi Shirley Lee^{1,2,3}, Olivier Buriez^{*4}, Eric Labbé⁴, Siden Top^{*2}, Pascal Pigeon¹, Gérard Jaouen¹, Christian Amatore^{*4}, and Weng Kee Leong³

¹ Chimie ParisTech, Ecole Nationale Supérieure de Chimie de Paris, 11 rue Pierre et Marie Curie, 75231 Paris Cedex 05, France

² Université Pierre et Marie Curie-Paris, Sorbonne Universités, Institut Parisien de Chimie Moléculaire (IPCM) - UMR 8232, 4, place Jussieu, 75252 Paris Cedex 05, France. tel: 33-1 44 27 66 99; e-mail, siden-top@chimie-paristech.fr.

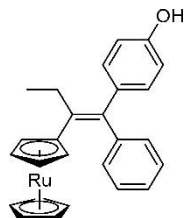
³ Division of Chemistry and Biological Chemistry, Nanyang Technological University, 21 Nanyang Link, Singapore 637371

⁴ Ecole Normale Supérieure - PSL Research University, Département de Chimie, Sorbonne Universités - UPMC Univ. Paris 06, CNRS UMR 8640 PASTEUR, 24 rue Lhomond, 75005 Paris, France. tel, 33-1 44 32 32 62; e-mail, olivier.buriez@ens.fr. tel, 33-1 44 32 33 88; e-mail, christian.amatore@ens.fr.

Abstract

The complete oxidation sequence of ruthenociphenol (**1**), an organometallic ruthenocene-based analogue of ferrocifens, a promising anticancer drug series, has been investigated by cyclic voltammetry. As for the unsubstituted ruthenocene, the oxidation of **1** produced the corresponding species **1**⁺, which engaged in a reversible dimerization reaction. The highest reversibility occurred in dichloromethane (DCM), a low-donor solvent, with the weakly coordinating supporting electrolyte anion B(C₆F₅)₄. Under these conditions, the addition of pyridine triggered a chemical sequence through which the hydroxyl group of electrogenerated **1**⁺ was ultimately converted into the phenoxy radical **2**. Unlike analogue ferrocifen derivatives, **2** did not undergo a further electrochemical oxidation but engaged in coupling with **1**⁺. The slow deprotonation of the resulting species appeared to be the key step leading to the quinone methide **3** after sluggish electron transfer. Again, in contrast with the ferrocifen series, **3** was not the final and stable complex of this oxidation sequence. It was indeed shown that the quinone methide spontaneously underwent a further oxidative evolution under our conditions. This led to a five-membered-ring closure and regeneration of the phenolic species

4, which could be further oxidized irreversibly, leading presumably to the new quinone methide 6. Such distinct behavior in comparison to ferrocene analogues may explain the different cytotoxic activities observed against hormone-independent breast cancer cells for ruthenocifens and ferrocifens.



1

Introduction

The use of metal compounds in drug development was stimulated by the discovery of the anticancerous activity of cisplatin.¹ A huge number of metal complexes have thus been extensively investigated, and some of them, such as NAMI-A² and KP1019,³ have entered clinical trials. Metal complex activity in medicinal chemistry can be viewed as forming two main categories depending on the role played by the metal, either as a reactive center (e.g., cisplatin),⁴ or as a scaffold enhancing the biological activity of a ligated molecule.⁵ The latter strategy is particularly well illustrated by “ferrocifens”, which are ferrocene derivatives of the efficient current breast cancer drug tamoxifen. Ferrocifen complexes express high antiproliferative activities against both hormone-dependent (ER+) and hormone-independent (ER-) breast cancer cells, in contrast to tamoxifen, which is only active against breast cancer cells displaying an estrogen receptor (ER+).⁶ On the basis of detailed electrochemical studies^{7,8} and biochemical oxidation metabolism,⁹ it was established that the activity of many ferrocifens involved the oxidative formation of cytotoxic quinone-type metabolites. These may then lock and deactivate target proteins or increase oxidative stress in cells, leading ultimately to their death.

Ruthenium complexes have a number of characteristics that make them suitable for development as antitumor metal complexes,¹⁰ including (i) the accessibility of oxidation states 2+, 3+, and 4+ under physiological conditions, (ii) the ability to tune electron transfer rates and redox potentials, (iii) the ability to mimic iron complexes in binding to biomolecules, and (iv) the availability of two γ -emitting isotopes, ⁹⁷Ru and ¹⁰³Ru, which may be useful for the radioimaging of cancer tumors.¹¹

A series of ruthenocene analogues of ferrocifens, based on the structure of tamoxifen, were prepared and tested *in vitro* against breast cancer cell lines to evaluate the importance of factors i–iv.¹² Interestingly, it was found that, unlike ferrocifens, these “ruthenocifens” acted as antiestrogens toward the ER+ breast cancer cells (MCF7) but had no cytotoxic effect on hormone-independent (ER-) MDA-MB-231 breast cancer cells when tested up to 1 μM . However, we have recently shown (*vide infra*) that the ruthenociphenol derivative **1** actually possesses an antiproliferative activity against the MDA-MB-231 cancer cells at higher concentrations ($\text{IC}_{50} = 4.01 \pm 1.8 \mu\text{M}$). In order to understand the lower activity observed with ruthenocifens compared to ferrocifens, their electrochemical behavior was investigated in methanol with Bu_4NBF_4 as the supporting electrolyte. Under such conditions, and in the absence of base, their cyclic voltammograms exhibited irreversible oxidation waves (in contrast to what was observed for ferrocifens), indicating a weaker stability of the electrogenerated cations in comparison to those obtained with the iron derivatives, in which the hole is mostly localized on the ferrocene moiety. Such behavior may be coherent with that of ruthenocene (Cp_2Ru), whose cation stability strongly depends on the nature of the solvent and of the supporting electrolyte.¹³ Geiger et al., in particular, showed that the electrochemical oxidation of ruthenocene in a low-donor solvent (CH_2Cl_2) with a weakly coordinating supporting electrolyte anion, such as tetrakis(perfluoroaryl)borate (TFAB), affords the dimeric dication $[(\text{RuCp}_2)_2]^{2+}$ in rapid equilibrium with the parent 17-electron ruthenocenium. Thus, at room temperature, a quasi-Nernstian cyclic voltammetry behavior was observed, whereas the oxidation displayed poor electrochemical reversibility at lower temperatures.^{13d,14} This prompted us to investigate the oxidative process of a ruthenocifen derivative as a function of the nature of the solvent and the supporting electrolyte.

The electrochemical behavior of the ruthenociphenol derivative **1** in acetonitrile and dichloromethane (DCM), with $[\text{nNBu}_4][\text{BF}_4]$ (=TBABF₄) or $[\text{nNBu}_4][\text{B}(\text{C}_6\text{F}_5)_4]$ (=TBA][TFAB]) as the supporting electrolyte, is first presented. The second part of the work is devoted to evaluating the electrochemical behavior of **1** in DCM/[TBA][TFAB] in the presence of pyridine as a model base which, as established for ferrociphenols, is required to trigger an oxidation sequence, affording ultimately the biologically active quinone methide. We thus expected that the presence of a pyridine base, as a model of basic biological moieties, could interfere with the spontaneous fate of the $[\text{Cp}_2\text{Ru}]^+$ center, so as to lead also to a quinone methide derivative. However, it is shown hereafter that the oxidative processes observed are more complex than for ferrocifens. A tentative mechanism is presented to

rationalize the voltammetric results, considering the sequential intermediates involved were too unstable to allow their chemical characterization.

Results and Discussion

General Synthesis and Antiproliferative Activity of **1**.

Ruthenociphenol **1** was prepared in 62% yield via a McMurry cross coupling, by a procedure similar to that reported for the ruthenocifen series.¹² It was successfully characterized by ¹H and ¹³C NMR spectroscopy and mass spectrometry, and the purity was checked by HPLC.

The antiproliferative activity of **1** was examined over a wide range of concentrations against the ER negative breast cancer cells MDA-MB-231. Its IC₅₀ value was found to be 4.01 ± 1.8 μM: i.e., higher but not excessively larger than that obtained for the ferrocenyl analogue of **1** (1.13 ± 0.07 μM).^{6f}

Electrochemical Behavior of Ruthenociphenol **1** as a Function of the Nature of the Solvent and the Supporting Electrolyte Anion

The cyclic voltammogram of **1**, in acetonitrile with TBABF₄ as the supporting electrolyte, obtained at a low scan rate, showed an irreversible wave at ca. +0.75 V and displayed a reduction system at +0.45 V during the backward scan, indicating that the electrogenerated ruthenocenium cation **1**⁺ was engaged in a dynamic chemical sequence (Figure 1).¹⁴ With respect to the electrochemical behavior of ruthenocene in the same solvent, the oxidation of **1** would involve two electrons.¹⁵ As already reported,¹⁶ the high electrophilicity of the electrogenerated Cp₂Ru⁺ moiety would favor a reaction with acetonitrile (MeCN) to give the corresponding (Cp₂Ru-MeCN)⁺ part which would be further oxidized at the potential value of **1** into (Cp₂Ru-MeCN)²⁺. Accordingly, the reduction wave at 0.45 V would feature the reduction of this dication.

In a low-donor solvent such as dichloromethane (DCM) the oxidation of **1** displayed a partially reversible monoelectronic wave (with respect to the peak current intensity of the bielectronic oxidation of **1** in acetonitrile) at 0.8 V. Replacing the supporting electrolyte anion by a weakly coordinating one (TFAB) afforded a reversible oxidation wave. However, this oxidation wave became irreversible either upon increasing the scan rate or decreasing the temperature of the solution (not shown). Both facts strongly suggested that under these latter conditions the one-electron reversible wave character was only apparent and involved a rapid

follow-up reversible dimerization, as reported previously for the parent ruthenocene¹³ or for a similar mechanism observed in organic electrochemistry.¹⁴

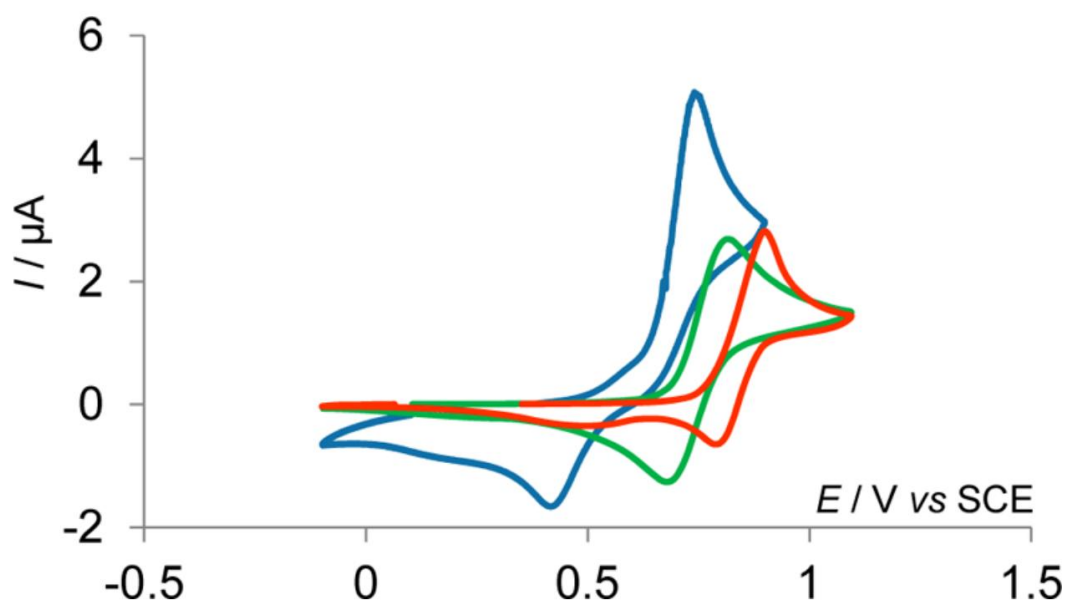
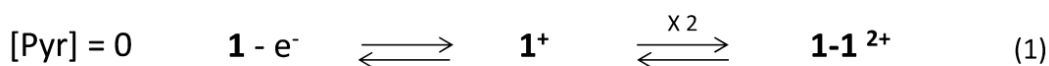
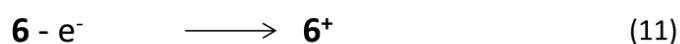
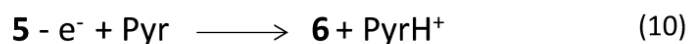
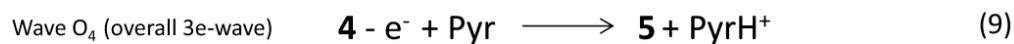
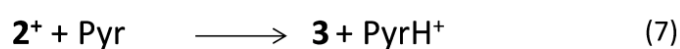
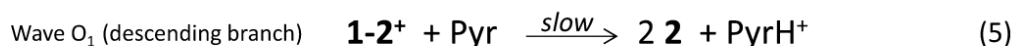
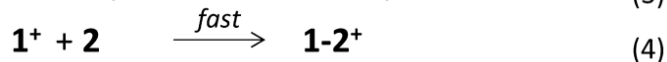
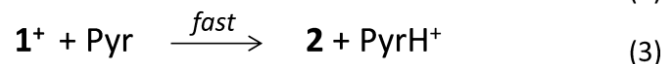
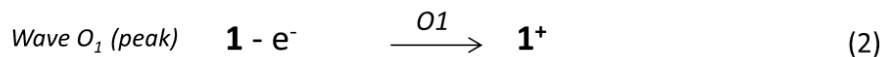


Figure 1. Cyclic voltammograms of **1** (2 mM) in (blue) acetonitrile/[TBA][BF₄] (*C* = 0.1 M), in (red) dichloromethane/[TBA][BF₄] (0.08 M), and in (green) dichloromethane/[TBA][TFAB] (0.08 M). Conditions: Pt electrode, 0.5 mm in diameter; scan rate 200 mV/s.

Indeed, this peculiar electrochemical behavior is consistent with an EC_{dim} mechanism in which, by analogy with ruthenocene,¹³ the chemical reaction following the electron transfer could be the dimerization of the ruthenocifen species **1**⁺ into a bis(ruthenocifen) dication (noted as **1-1**²⁺ in Scheme 1). The quasi-Nernstian shape of the cyclic voltammogram obtained at low scan rate and in DCM/[TBA][TFAB] is in agreement with a fast and reversible dimerization process.¹⁴ Similar to the case of Cp₂Ru, the electrochemical reduction of this dimer would take place through the wave located at +0.5 V unless the rate of the dynamic equilibrium was fast enough (highest temperature, lowest scan rates) for the dimerization to be pulled back through the reduction of **1**⁺.¹⁴ Such results evidenced that, if a base could interact with the tamoxifen ligand in **1**⁺, it may induce a pathway similar to that evidenced for ferrociphenols by pulling back the dimerization equilibrium.⁷⁻⁹ For these reasons we wished to investigate the reactivity of **1**⁺ toward pyridine in DCM/[TBA][TFAB] in order to allow such a pathway to occur easily.

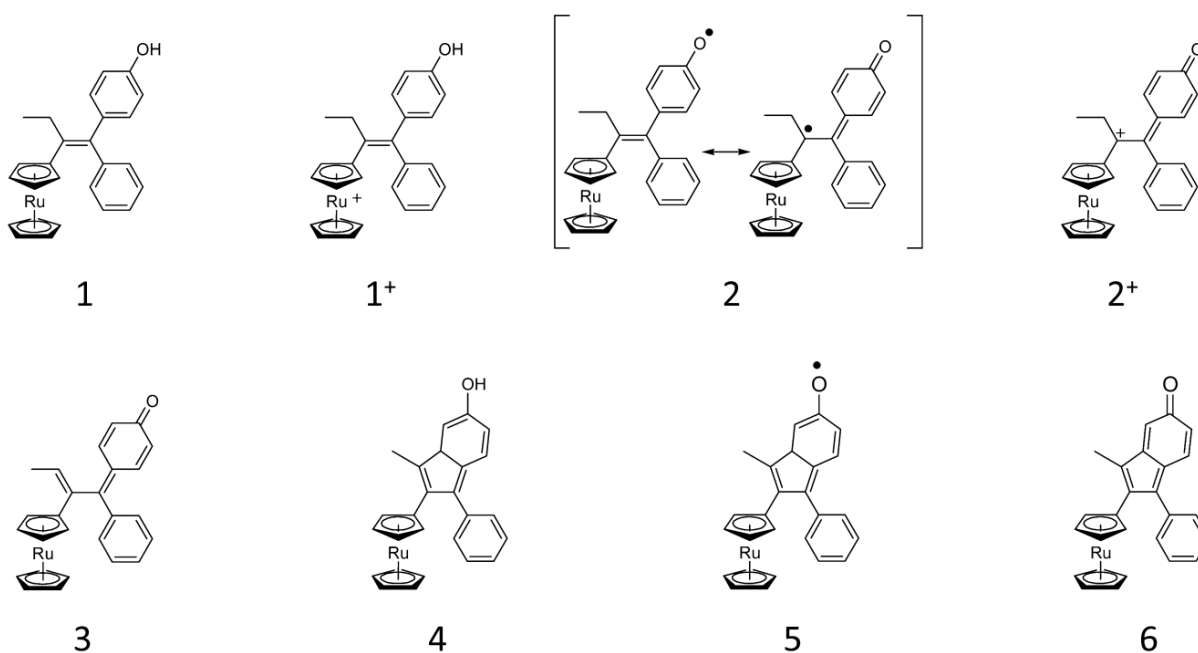


$[\text{Pyr}] \neq 0$



Scheme 1. Full Oxidation Sequence of **1** in the Absence and the Presence of Pyridine as a Base^a

^a See the corresponding structures in Scheme 2. No potential structure is postulated for species **1-2**⁺, but it may be similar to that of $[\text{RuCp}_2]_2^{2+}$.¹³



Scheme 2. Chemical Structures of the Main Complexes Involved in the Oxidation Sequence of **1** in the Absence and the Presence of Pyridine^a

^a See Scheme 1.

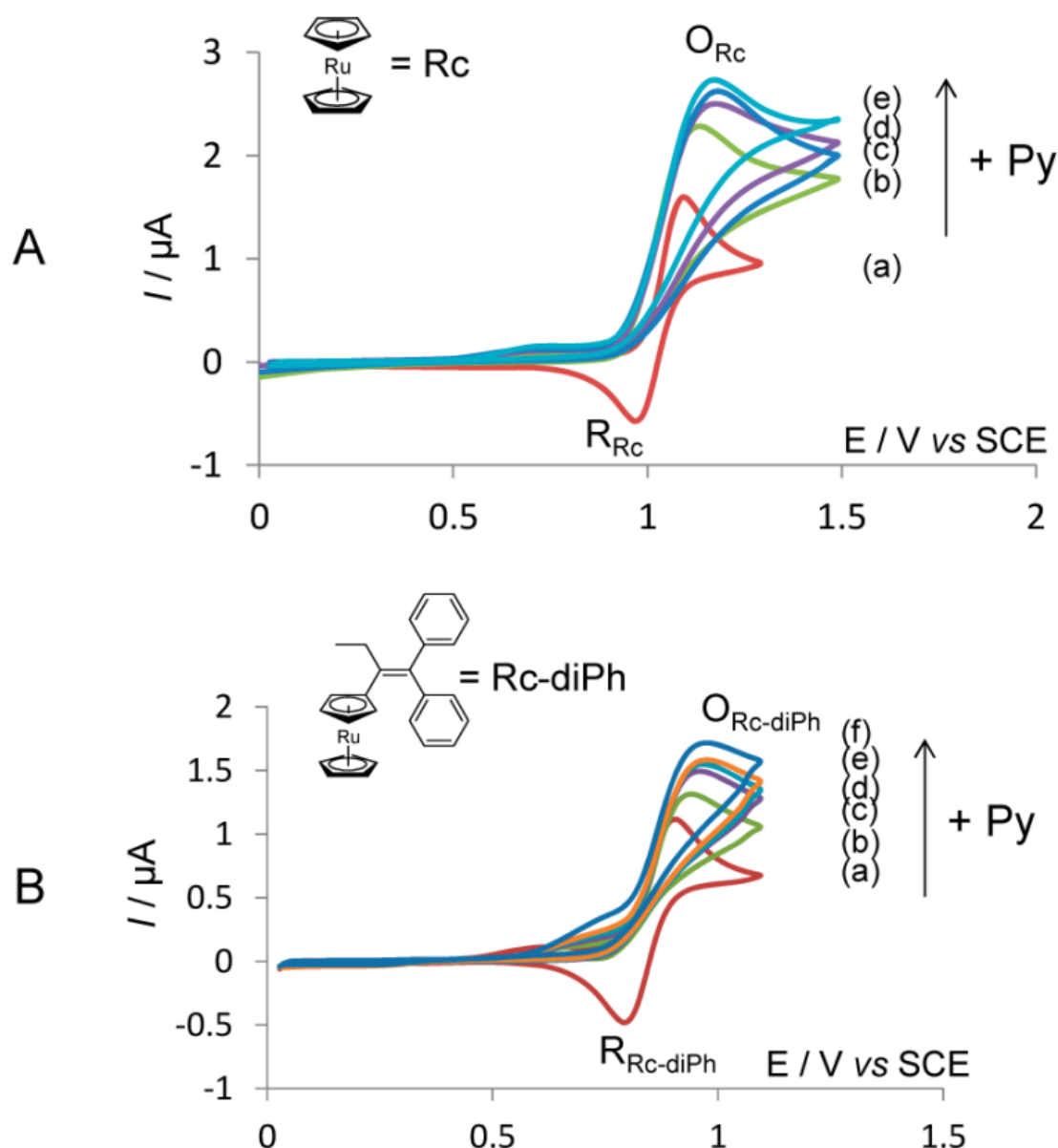


Figure 2. (A) Cyclic voltammograms of Rc (2 mM) in the absence (a) and the presence of increasing amounts of pyridine (2 (b), 4 (c), 10 (d), and 20 mM (e), respectively). (B) Cyclic voltammograms of Rc-diPh (1 mM) in the absence (a) and the presence of increasing amounts of pyridine (2 (b), 10 (c), 20 (d), 40 (e), and 100 mM (f), respectively). Conditions: studies performed in DCM/[TBA][TFAB] (0.08 M); Pt electrode, 0.5 mm in diameter; scan rate 100 mV/s.

Electrochemical Behavior of **1** in DCM/[TBA][TFAB] in the Presence of Pyridine

Since the reactivity of the electrogenerated 1^+ species strongly depends on its environment (solvent, supporting electrolyte), we first reinvestigated the electrochemical behavior of ruthenocene (Rc) and examined that of a nonphenolic ruthenocifen (Rc-diPh; see Figure 2) in the presence of pyridine to obtain some reference behaviors. In the absence of base, both compounds exhibited a reversible oxidation wave in DCM/[TBA][TFAB], as observed for the

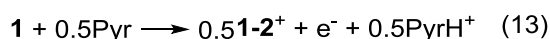
ruthenociphenol complex **1** (Figure 2). Nevertheless, the oxidation process of Rc-diPh occurred at a potential value less positive than that for Rc, indicating an electron-donating effect of the organic fragment attached onto the Cp ring. Upon addition of 1 molar equiv of pyridine used as a model of a nucleophilic base, the oxidation wave of ruthenocene became fully irreversible, whereas its peak current intensity increased concomitantly. Additionally, the oxidation wave was broad, in agreement with a rather sluggish displacement of the $[\text{Cp}_2\text{Ru}]_2^{2+}$ species by the pyridine. In the presence of excess pyridine, the oxidation wave doubled in size, indicating the occurrence of an ECE mechanism (Figure 2A). By analogy with the reactivity of ruthenocenium with nucleophiles (Cl^- , MeCN, THF),¹⁶ this suggests that the electrogenerated 17-electron species reacts with pyridine to give the corresponding $(\text{Cp}_2\text{Ru-Py})^+$ complex, which is oxidized at a similar potential value into the 18-electron dication $(\text{Cp}_2\text{Ru-Py})^{2+}$. Indeed, the susceptibility of Cp_2Ru^+ toward nucleophilic attack (and/or dimerization) has been reported with other nucleophiles and ascribed to the large ring–ring separation.^{13b,17} Interestingly, at high pyridine excesses a small current plateau is observable before the main wave ($E_{1/2}$ at ca. 0.65 V), suggesting the occurrence of a CE-type mechanism corresponding to the fact that pyridine may weakly interact with the Cp_2Ru moiety prior to its oxidation.

A similar electrochemical behavior was observed with the ruthenocifen derivative Rc-diPh, though the peak current increase of the oxidation wave with the base concentration was smaller than for Rc (Figure 2B). Interestingly, the CE-type minor path noted for Cp_2Ru was also noted here, suggesting that the uphill interaction between pyridine and the Cp_2Ru moiety is conserved in Rc-diPh. However, the major pathway involved the reaction of the electrogenerated $(\text{Rc-diPh})^+$ with pyridine leading to an ECE process, though being less efficient than for Rc, showing again that the presence of the organic moiety on the Cp ring induces rather large distortions of the Cp_2Ru cation reactivity. Again, this ECE mechanism featured the passage from an apparently diffusion controlled shape for the oxidation wave in the absence of pyridine to a more horizontal “plateau” shape of the oxidation wave when pyridine was added. This behavior shows that the reaction with pyridine is slower than the dimerization of $(\text{Rc-diPh})^+$ and continues to proceed after the wave peak.

Even if it is different in the nature of the reactions involved, the oxidation of **1** in the presence of pyridine displayed similar electrochemical features. The oxidation wave of **1** (noted as O_1) became fully irreversible upon addition of 1 molar equiv of pyridine (note that for clarity the various waves are labeled with subscripts identical with the label of the species shown in

Scheme 2 rather than in the order of their detection). However, the oxidation wave shifted toward a less positive potential value, indicating a very fast reaction between $\mathbf{1}^+$ and pyridine in comparison to Rc^+ and Rc-diPh^+ (Figure 3A). This behavior, by analogy to that obtained with ferrociphenol derivatives, could be ascribed to a deprotonation of the hydroxyl group. As suggested by the important displacement of the oxidation wave toward less positive potential values, the possible competitive nucleophilic attack of pyridine on the Ru metal center (as for Rc or Rc-diPh) may certainly be disregarded. However, in view of the ferrocene analogue, it was highly surprising to observe that such a facile reaction of $\mathbf{1}^+$ did not lead to the expected ECE sequence, viz. to a doubling of the current peak intensity,¹⁸ since the current peak of wave O_1 remained nearly monoelectronic. This evidenced the occurrence of an unexpected follow-up process for $\mathbf{2}$, preventing its oxidation (ECC-type mechanism). In keeping with the previously described reactivity of ruthenocenium species, the radical species $\mathbf{2}$ could react with $\mathbf{1}^+$ to produce the corresponding dimeric species $\mathbf{1-2}^+$, which would reduce at wave R_2 during the backward scan (see the “(2)–(4)” sequence in Scheme 1). Actually, the formation of $\mathbf{1-2}^+$ - rather than considering a possible radical–radical coupling of $\mathbf{2}$ - is consistent with (i) the probable cationic character of the species which reduces at wave R_2 , as observed for ferrocifens in the same potential region¹⁸ or for $(\text{Rc})_2^{2+}$,¹³ and (ii) the reactivity of the species toward pyridine (see below), which suggests that an acidic (phenolic) proton is still present.

Thus, the formation of $\mathbf{1-2}^+$ through the (2) + (3) + (4) pathway in Scheme 1 results in an overall monoelectronic oxidation of $\mathbf{1}$ according to



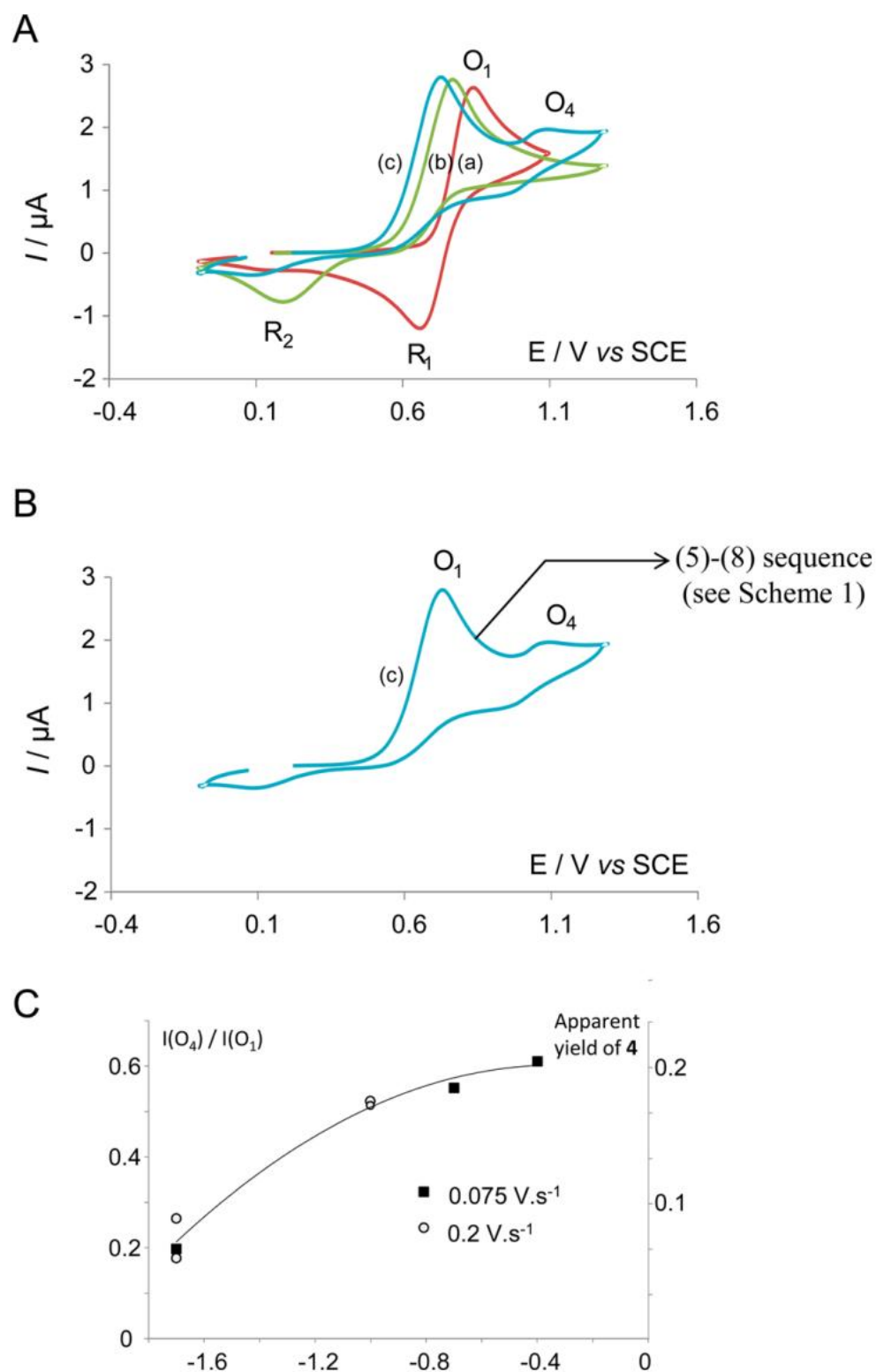


Figure 3. (A) Cyclic voltammograms of **1** (2 mM) in the absence (a) and the presence of pyridine (2 (b) and 20 mM (c), respectively). Conditions: study performed in DCM/[TBA][TFAB] (0.08 M); Pt electrode, 0.5 mm in diameter; scan rate 200 mV/s. (B) Cyclic voltammogram (c) isolated from part A and showing the chemical sequence occurring in the descending branch of wave O_1 (from Scheme 1). (C) Variation of $I(O_4)/I(O_1)$ (peak current ratio between waves O_4 and O_1 , left vertical axis) and of y_{O_4} (apparent yield for compound **4**, right vertical axis) as a function of the logarithm of pyridine concentration at two scan rates.

At higher pyridine concentrations, the new oxidation wave O_4 was observed at more positive potential value, whereas R_2 disappeared within the same time scale (Figure 3A). We primarily envisioned that wave O_4 represented the oxidation of the quinone methide formed through the three-electron reactive cascade (2)–(7) initiated by the deprotonation of 1^+ by pyridine (Scheme 1). However, Figure 4 shows that the oxidation of an authentic sample of quinone methide **3** (prepared by the chemical oxidation of **1** with Ag_2O) occurred at wave O_3 , located between waves O_1 and O_4 , while no trace of wave O_3 could be observed within the scan rate range used in this work (compare parts A and B of Figure 4).

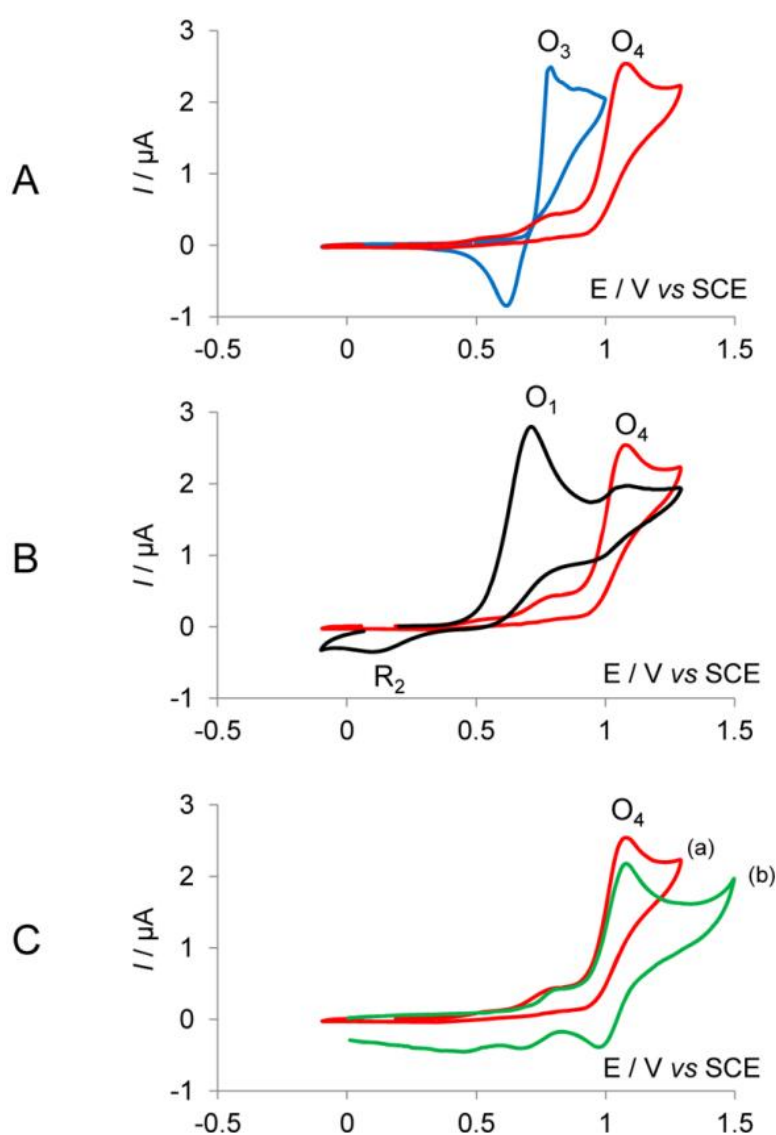
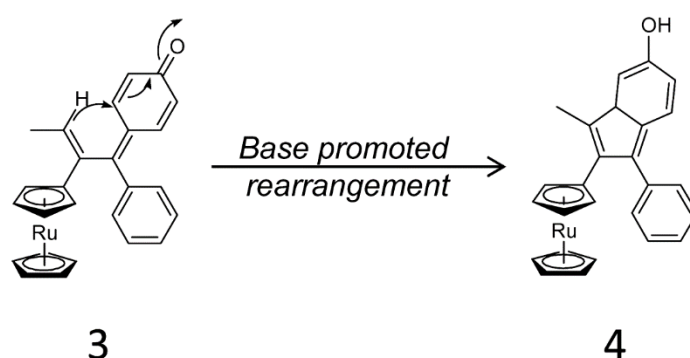


Figure 4. (A) Cyclic voltammograms of the quinone methide **3** (2 mM) in 0.08 M DCM/[TBA][TFAB] in the absence (blue curve) and in the presence (red curve) of 2 mM pyridine. (B) Superimposition of the cyclic voltammograms of **1** (2 mM) obtained in the presence of 20 mM pyridine and of the quinone methide **3** (2 mM) in the presence of 2 mM pyridine. (C) Superimposition of voltammograms obtained from the quinone

methide **3** (2 mM) in the presence of 2 mM pyridine (a) and of **4** in the absence of pyridine (b). To allow a better comparison between (a) and (b), the current of **4** (initially obtained for 0.8 mM) was multiplied by a factor of 3. Conditions: DCM/[TBA][TFAB] (0.08 M); Pt electrode, 0.5 mm in diameter; scan rate 200 mV/s.

An authentic sample of **3** was left to react with sodium hydroxide (see the Experimental Section) and analyzed electrochemically. This effectively led to the observation of wave O₄ (Figure 4C). Moreover, this wave was also observed when the quinone methide was electrochemically oxidized in the presence of pyridine (Figure 4A). It could then be safely concluded that wave O₄ represents the oxidation of the cyclized derivative **4** most likely formed through a base-promoted rearrangement of **3** (Scheme 3).



Scheme 3.

Figure 3B reports the current peak ratio between waves O₄ and O₁ and is converted into an apparent yield for **4**, assuming that the oxidation of **4** involves a three-electron process (reactions (9)–(11) in Scheme 1). However, the follow-up products obtained from **4** may undergo coupling as well to yield nonelectroactive products (compare the absence of reduction peaks in the backward trace of O₄ wave in Figure 4C(a)). Indeed, in the absence of pyridine (Figure 4C(b)) cathodic waves appeared which may be ascribed to coupling cationic products by analogy to RuCp₂ oxidation.¹³ In partial support of such a parallel pathway it was noted that scanning beyond wave O₄ at large pyridine excesses led to significant electrode clogging. Therefore, the apparent yield for **4** reported in Figure 3B is the minimal one and the actual yield y_{O_4} may be comprised between y_{O_4} and xy_{O_4} , where x is smaller than 3 and may depend on the pyridine concentration.

As shown in Figure 4C, the oxidation of complex **4** is reversible in the absence of base, whereas no reversibility was observed in the presence of pyridine. Here again, this behavior is very likely due to the deprotonation of the hydroxyl group from **4**⁺, a process that should

initiate a cascade leading to the cyclized quinone methide **6** (reactions (9)–(11) in Scheme 1). Unfortunately, the low yield of **6** prevented its characterization. Nevertheless, within this framework wave O₄ involves three electrons per molecule of **4**. This shows that its current peak relative to that of wave O₁ in Figure 3A(c) corresponds to ca. 10%.

Since wave O₄ corresponds to the electrochemical signature of compound **4** formed at large pyridine concentrations (Figure 3A(c)), it also represents the electrochemically observable result of the overall kinetics of the oxidation process: i.e., through the full (2)–(8) sequence in Scheme 1. Thus, the intermediate oxidation step required to convert **1-2**⁺ into **4** (labeled (6) in Scheme 1) must proceed within the time elapsed while scanning the potential between wave O₁ and wave O₄: i.e., within a few seconds with respect to the scan rates used. This is somehow consistent with the not strictly diffusional shape of wave O₁ at large pyridine concentration: viz., the postpeak current never decays as fast as what would be expected for a diffusion-controlled process (compare curve (c) to curve (a) in Figure 3A), featuring the pyridine-promoted cascade of oxidation steps (5)–(8) (Figure 3B). Owing to the low maximum yield in **4** observed in Figure 3B, it is perfectly reasonable that the increase of the peak descending branch is sufficient to account for the required charge.

Therefore, the oxidation sequence of ruthenocifen **1** follows a different pathway with respect to that depicted for ferrocifens. First, the ultimate stable oxidation product at wave O₁ is **4**, which is formed along a three-electron process but in a very moderate yield due to the one-electron formation of dimer **1-2**⁺, the deprotonation of which is the rate-determining step of the entire follow-up oxidation sequence.

Conclusions

The general oxidation sequence of ruthenociphenol **1** could be anticipated as being similar to that of the analogue ferrociphenol. However, some important differences could be established. First, it was shown that deprotonation of the hydroxyl group in **1** was more efficient than a possible nucleophilic attack of the pyridine on the Ru metal center. Second, the phenoxy radical **2** produced after deprotonation of the electrogenerated **1**⁺ was not electrochemically oxidized but most likely engaged in a chemical process leading to a dimeric species. Third, the quinone methide **3** was unstable in basic media; it underwent further evolution due to the increased acidity of the hydrogen located on the allylic carbon compared to the ferrocifen-derived analogue. Finally, the subsequent oxidation pathway is kinetically controlled by the

deprotonation of the dimeric species. These differences observed between the ruthenocene and ferrocene derivatives, and notably the instability of the quinone methide, may explain their different cytotoxic activities against breast cancer cells.

Experimental Section

Cyclic Voltammetry Experiments

Cyclic voltammetry experiments were performed at room temperature under an argon atmosphere in a three-electrode cell by using an Autolab potentiostat (PGSTAT 20). The reference electrode was an SCE (saturated calomel electrode; Tacussel), which was separated from the solution by a bridge compartment filled with the same solvent/supporting electrolyte solution as used in the cell. The counter electrode was a platinum grid (ca. 0.5 cm², Goodfellow). The glass-sealed platinum working electrode disks (0.5 mm diameter, Goodfellow) were homemade.

Syntheses

Except for **1**, **3**, and **4**, whose characterizations are reported below, all other products involved in the mechanism reported in Scheme 1 were too unstable to be obtained by preparative electrolyses; therefore, they were only postulated due to kinetic requirements based on the specific voltammetric evidence and previous reactivities of analogous parent species.^{13,18}

Synthetic steps were carried out under an atmosphere of argon using standard Schlenk techniques. ¹H and ¹³C NMR spectra were recorded on a Bruker 300 NMR spectrometer as *d*₆-acetone solutions; chemical shifts reported were referenced against the residual proton signals of the solvent. Mass spectra (MS) were obtained on DSQII and ITQ 110 Thermo Scientific spectrometers by electronic impact (EI) and chemical ionization (CI) methods. IC₅₀ values of **1** on MDA-MB-231 breast cancer cells were performed by ImaGIF Ciblotheque Cellulaire (Institut de Chimie des Substances Naturelles). The procedure is described in ref 19. TBA⁺B(C₆F₄)⁻ electrolyte was synthesized according to the literature;¹³ all other chemicals were purchased from commercial sources and used as supplied.

Synthesis of Ruthenociphenol **1**

TiCl₄ (0.46 mL, 4.17 mmol) was added to a suspension of zinc powder (545 mg, 8.34 mmol) in THF (8 mL) in an ice bath. The mixture was then heated at reflux for 1 h to give a dark blue mixture. A second solution was prepared by dissolving 4-hydroxybenzophenone (413

mg, 2.08 mmol) and propionyl ruthenocene (400 mg, 1.39 mmol) in THF (2 mL). This latter solution was added to the first solution, and the resulting mixture was heated for 2 h. After it was cooled to room temperature, the mixture was hydrolyzed with water (30 mL). After extraction with dichloromethane and solvent removal, the crude product was purified by column chromatography with petroleum ether/ether (2/1, v/v) as eluent. Yield: 392 mg (62%). ¹H NMR (300 MHz, CD₃COCD₃; *Z* + *E* isomers): δ 0.99 + 1.02 (t, t, 3H, *J* = 7.5 Hz, CH₃, *Z* isomer + *E* isomer), 2.36 + 2.38 (q, q, 2H, *J* = 7.5 Hz, CH₂, *Z* isomer + *E* isomer), 4.26 (t, 1H, *J* = 1.7 Hz, C₅H₄), 4.33 (t, 1H, *J* = 1.5 Hz, C₅H₄), 4.36 (t, 1H, *J* = 1.5 Hz, C₅H₄), 4.40 (t, 1H, *J* = 1.5 Hz, C₅H₄), 4.52 + 4.53 (s, s, 5H, C₅H₅, *Z* isomer + *E* isomer), 6.70 + 6.80 + 6.90 + 7.01 (4 d, 2H, *J* = 8.7 Hz, C₆H₄, *Z* isomer + *E* isomer), 7.01–7.24 (m, 3H, C₆H₅), 7.31 (t, 2H, C₆H₅), 8.25 (s, 1H, OH). ¹³C NMR (75.45 MHz, CD₃COCD₃): δ 15.9 (CH₃), 29.7 + 29.8 (CH₂), 70.4 (2CH, C₅H₄), 71.8 (5CH, C₅H₅), 72.6 (2CH, C₅H₄), 92.9 (C, C₅H₄), 115.7 + 115.8, 128.7 + 129.0, 130.0, 131.0, 131.7 (CH, Ar), 126.8 + 126.9 (CH_p of C₆H₅), 136.4 (C), 136.6 (C), 136.8 (C), 138.9 (C), 139.0 (C), 145.7 (C), 146.0 (C), 156.8 (C-OH). EI-MS: 454.5 [M]⁺. Anal. Calcd for C₂₆H₂₄ORu: C, 68.85; H, 5.33. Found: C, 68.57; H, 5.37.

Synthesis of Ruthenocenyl Quinone Methide 3

Ruthenociphenol (40 mg, 0.088 mmol) was first dissolved in anhydrous acetone (3 mL) in a Schlenk vessel. Ag₂O (62 mg, 0.26 mmol) was added, and the solution was stirred at room temperature for 3 h. The reaction mixture was then centrifuged (4000 rpm, 6 min), decanted, and vacuum-dried. The product was purified by column chromatography using diethyl ether/petroleum ether (2/1, v/v) as eluent. Yield: 36 mg (90%) ¹H NMR (300 MHz, CD₃COCD₃): δ 1.53 (d, 3H, *J* = 7.0 Hz, CH₃, major isomer), 1.96 (d, 3H, *J* = 7.0 Hz, CH₃, minor isomer), 4.25 (s, 5H, C₅H₅, major isomer), 4.18–4.40 (m, 4H, C₅H₄), 4.40 (s, 5H, C₅H₅, minor isomer), 5.63 (q, 1H, *J* = 7.0 Hz, *CH*-Me, minor isomer), 6.23 (q, 1H, *J* = 7.0 Hz, *CH*-Me, major isomer), 6.20–6.33 (m, 2H, C₆H₄), 7.24–7.53 (m, 8H, C₆H₅ + C₆H₄). ¹³C NMR (75.45 MHz, CD₃COCD₃): δ: 15.7 (CH₃, major isomer), 16.2 (CH₃, minor isomer), 30.6 (*CH*-Me, major isomer), 29.8 (*CH*-Me, major isomer), (69.8 + 70.7 + 71.0 + 72.9 (C₅H₄), 72.0 (C₅H₅, major isomer), 72.1 (C₅H₅, minor isomer), 92.4 (C, C₅H₅), 125.4 (CH₃-CH=C), 129.2, 129.4, 129.8, 130.8, 131.6, 138.2 + 140.0 (CH of C₆H₅ and C₆H₄), 129.3 (C), 130.5 (C), 137.9 (C), 138.7 (C), 157.3 (C), 186.8 (C=O). EI-MS: 452.2 [M]⁺. Anal. Calcd for C₂₆H₂₂ORu: C, 69.16; H, 4.91. Found: C, 69.29; H, 5.03.

Synthesis of 1,1-Diphenyl-2-ruthenocenyl-but-1-ene (=Rc-diPh)

TiCl₄ (0.96 mL, 8.7 mmol) was added to a suspension of zinc powder (796 mg, 12.2 mmol) in THF (8 mL) in an ice bath. The mixture was then heated at reflux for 2 h to obtain a dark blue mixture. A second solution was prepared by dissolving benzophenone (476 mg, 2.6 mmol) and propionyl ruthenocene (500 mg, 1.74 mmol) in THF (6 mL). This latter solution was added to the first solution, and the resulting mixture was heated for 2 h. After it was cooled to room temperature, the mixture was hydrolyzed with water (20 mL). After extraction with dichloromethane and solvent removal, the crude product was purified by preparative HPLC using acetonitrile as eluent. Yield: 46%. ¹H NMR (300 MHz, CDCl₃): δ 0.93 (t, 3H, *J* = 7.5 Hz, CH₃), 2.26 (q, 2H, *J* = 7.5 Hz, CH₃), 4.22 (t, 2H, *J* = 1.6 Hz, C₅H₄), 4.32 (t, 2H, *J* = 1.6 Hz, C₅H₄), 4.45 (s, 5H, Cp), 6.94–7.33 (m, 10H, C₆H₅). ¹³C NMR (75.45 MHz, CDCl₃): δ 15.6 (CH₃), 29.2 (CH₂), 69.8 (2CH, C₅H₄), 71.1 (5CH, C₅H₅), 72.0 (2CH, C₅H₄), 92.1 (C, C₅H₄), 121.1 (CH, Ph), 126.2 (CH, Ph), 128.0 (2CH, Ph), 128.2 (2CH, Ph), 129.3 (2CH, Ph), 129.9 (2CH, Ph), 136.4 (C), 138.2 (C), 144.2 (C), 144.4 (C). Cl-MS: 439.2 [M + H]⁺. Anal. Calcd for C₂₆H₂₄Ru: C, 71.37; H, 5.53. Found: C, 71.14; H, 5.52.

Attempted Reaction of 3 and Base

Ruthenocenyl quinone methide **3** (100 mg, 0.22 mmol) was placed with DMF (5 mL) in a Schlenk vessel, followed by the addition of NaOH (10 mg, 0.24 mmol). The mixture was heated to 50 °C with stirring for 3 h. The reaction mixture was then hydrolyzed with water (5 mL) and extracted with ethyl acetate (3 × 20 mL). The crude mixture was dried over MgSO₄, concentrated, and purified by column chromatography using diethyl ether/petroleum ether (2/1, v/v) as the eluent. Yield of product **4**: 10 mg (10%). ¹H NMR (300 MHz, CD₃COCD₃): δ 1.89 (s, 3H, CH₃), 4.03–4.04 (m, 1H, C₅H₄), 4.37–4.39 (m, 1H, C₅H₄), 4.51–4.54 (m, 6H, C₅H₅ + C₅H₄), 4.84–4.85 (m, 1H, C₅H₄), 5.60 (s, 1H, OH), 5.91–5.96 (m, 2H, C₆H₄), 6.91–6.95 (dd, 1H, *J* = 2.6 Hz, 3.3 Hz, C₆H₄), 7.01–7.06 (dd, 1H, *J* = 2.6 Hz, 3.3 Hz, C₆H₄), 7.11–7.39 (m, 5H, C₆H₅).

Notes The authors declare no competing financial interest.

Acknowledgment

The authors thank the Agence Nationale de la Recherche for financial support (Mecaferrol) of S.T., the Nanyang Technological University through a start-up grant (Grant no. M4080504) to W.K.L., and the NTU-ParisTech joint Ph.D. Programme for a Research Scholarship to

H.Z.S.L. This work was also supported by the CNRS (UMR 8640), the Ecole Normale Supérieure, and the University P. et M. Curie.

References

- 1 (a) Rosenberg, B.; Vancamp, L.; Krigas, T. *Nature*. **1965**, *205*, 698. (b) Rosenberg, B.; Vancamp, L.; Trosko, J. E.; Mansour, V. H. *Nature*. **1969**, *222*, 385. (c) Hartinger, C. G.; Dyson, P. *J. Chem. Soc. Rev.* **2009**, *38*, 391.
- 2 (a) Alessio, E.; Mestroni, G.; Bergamo, A.; Sava, G. *Curr. Top. Med. Chem.* **2004**, *4*, 1525. (b) Bergamo, A.; Gaiddon, C.; Schellens, J. H. M.; Beijnen, J. H.; Sava, G. *J. Inorg. Biochem.* **2012**, *106*, 90. (c) Rademaker-Lakhai, J. M.; Van der Bongard, D.; Pluim, D.; Beijnen, J. H.; Schellens, J. H. M. *Clin. Cancer Res.* **2004**, *10*, 3717.
- 3 (a) Kopf-Maier, P. *Anticancer Res.* **1999**, *19*, 493. (b) Korfel, A.; Scheulen, M. E.; Schmoll, H. J.; Grundel, O.; Harstick, A.; Knoche, M.; Fels, L. M.; Skorzec, M.; Bach, F.; Baumgart, J.; Saß, G.; Seeber, S.; Thiel, E.; Berdel, W. E. *Clin. Cancer Res.* **1998**, *4*, 2701. (c) Kroger, N.; Kleeberg, U. R.; Mross, K.; Edler, L.; Hossfeld, D. K. *Onkologie* **2000**, *23*, 60.
- 4 (a) Jakupec, M. A.; Galanski, M.; Arion, V. B.; Hartinger, C. G.; Keppler, B. K. *Dalton Trans.* **2008**, 183. (b) Jakupec, M. A.; Keppler, B. K. *Curr. Topics Med. Chem.* **2004**, *4*, 1575. (c) Alessio, E.; Mestroni, G.; Bergamo, A.; Sava, G.; Sigel, A.; Sigel, H. *Met. Ions Biol. Syst.* **2004**, *42*, 323.
- 5 (a) Dubar, F.; Egan, T. J.; Pradines, B.; Kuter, D.; Ncokazi, K. K.; Forge, D.; Paul, J. F.; Pierrot, C.; Kalamou, H.; Khalife, J.; Buisine, E.; Rogier, C.; Vezin, H.; Forfar, I.; Slomianny, C.; Trivelli, X.; Kapishnikov, S.; Leiserowitz, L.; Dive, D.; Biot, C. *ACS Chem. Biol.* **2011**, *6*, 275. (b) Dubar, F.; Khalife, J.; Brocard, J.; Dive, D.; Biot, C. *Molecules* **2008**, *13*, 2900. (c) Ott, I.; Kircher, B.; Bagowski, C. P.; Vlecken, D. H. W.; Ott, E. B.; Will, J.; Bensdorf, K.; Sheldrick, W. S.; Gust, R. *Angew. Chem., Int. Ed.* **2009**, *48*, 1160. (d) Meggers, E. *Chem. Commun.* **2009**, *9*, 1001. (e) Vessières, A.; Top, S.; Pigeon, P.; Hillard, E. A.; Boubeker, L.; Spera, D.; Jaouen, G. *J. Med. Chem.* **2005**, *48*, 12. (f) Jaouen, G.; Top, S.; Vessières, A. In *Bioorganometallics*; Jaouen, G., Ed.; Wiley-VCH: Weinheim, Germany, 2006; p 65.
- 6 (a) Hillard, E. A.; Vessières, A.; Jaouen, G. In *Medicinal Organometallic Chemistry*; Jaouen, G., Metzler-Nolte, N., Eds.; Springer: Heidelberg, Germany, 2010; Vol. 32, pp 81–117. (b) Nguyen, A.; Vessières, A.; Hillard, E. A.; Top, S.; Pigeon, P.; Jaouen, G.

- Chimia*. **2007**, *61*, 716. (c) Vessières, A. *J. Organomet. Chem.* **2013**, *734*, 3. (d) Top, S.; Vessières, A.; Leclercq, G.; Quivy, J.; Tang, J.; Vaissermann, J.; Huché, M.; Jaouen, G. *Chem. Eur. J.* **2003**, *9*, 5223. (e) Top, S.; Vessières, A.; Cabestaing, C.; Laios, I.; Leclercq, G.; Provot, C.; Jaouen, G. *J. Organomet. Chem.* **2001**, *637*, 500. (f) Hillard, E. A.; Pigeon, P.; Vessières, A.; Amatore, A.; Jaouen, G. *Dalton Trans.* **2007**, 5073.
- 7 (a) Hillard, E. A.; Vessières, A.; Thouin, L.; Jaouen, G.; Amatore, C. *Angew. Chem., Int. Ed.* **2006**, *45*, 285. (b) Pigeon, P.; Top, S.; Zekri, O.; Hillard, E. A.; Vessières, A.; Plamont, M. A.; Buriez, O.; Labbé, E.; Huché, M.; Boutamine, S.; Amatore, C.; Jaouen, G. *J. Organomet. Chem.* **2009**, *694*, 895. (c) Tan, Y. L. K.; Pigeon, P.; Top, S.; Labbé, E.; Buriez, O.; Hillard, E. A.; Vessières, A.; Amatore, C.; Leonge, W. K.; Jaouen, G. *Dalton Trans.* **2012**, *41*, 7537. (d) Cazares-Marinero, J. d. J.; Labbé, E.; Top, S.; Buriez, O.; Amatore, C.; Jaouen, G. *J. Organomet. Chem.* **2013**, *744*, 92–100. (e) Cazares-Marinero, J. de J.; Buriez, O.; Labbé, E.; Top, S.; Amatore, C.; Jaouen, G. *Organometallics* **2013**, *32*, 5926–5934.
- 8 (a) Buriez, O.; Heldt, J. M.; Labbé, E.; Vessières, A.; Jaouen, G.; Amatore, C. *Chem. Eur. J.* **2008**, *14*, 8195. (b) Buriez, O.; Labbé, E.; Pigeon, P.; Jaouen, G.; Amatore, C. *J. Electronanal. Chem.* **2008**, *619*, 169. (c) Mertins, O.; Buriez, O.; Labbé, E.; Fang, P.-P.; Hillard, E. A.; Vessières, A.; Jaouen, G.; Tian, Z.-K.; Amatore, C. *J. Electroanal. Chem.* **2009**, *635*, 13. (d) Mertins, O.; Messina, P.; Labbé, E.; Vivier, V.; Arbault, S.; Lemaitre, F.; Buriez, O.; Amatore, C. *Inorg. Chim. Acta* **2011**, *374*, 59.
- 9 Hamels, D.; Dansette, P. M.; Hillard, E. A.; Top, S.; Vessières, A.; Herson, P.; Jaouen, G.; Mansuy, D. *Angew. Chem.* **2009**, *121*, 9288; *Angew. Chem., Int. Ed.* **2009**, *48*, 9124.
- 10 (a) Clarke, M. *J. Coord. Chem. Rev.* **2003**, *236*, 209. (b) Allardyce, C. S.; Dyson, P. J. *Platinum Met. Rev.* **2001**, *45*, 62.
- 11 (a) Taylor, A. J.; Wenzel, M. *Xenobiotica* **1978**, *8*, 107. (b) Wenzel, M.; Asindraza, P.; Schachschneider, G. *J. Labelled Compd. Radiopharm.* **1983**, *20*, 1061–1071. (c) Stadlbauer, E.; Nipper, E.; Wenzel, M. *J. Labelled Compd. Radiopharm.* **1977**, *13*, 491. (d) Hoffmann, K.; Riesselmann, B.; Wenzel, M. *J. Labelled Compd.* **1980**, *17*, 421.
- 12 (a) Pigeon, P.; Top, S.; Vessières, A.; Huché, M.; Hillard, E. A.; Salomon, E.; Jaouen, G. *J. Med. Chem.* **2005**, *48*, 2814. (b) Hillard, E. A.; Vessières, A.; Top, S.; Pigeon, P.; Kowalski, K.; Huché, M.; Jaouen, G. *J. Organomet. Chem.* **2007**, *692*, 1315.

- 13 (a) Swarts, J. C.; Nafady, A.; Roudebush, J. H.; Trupia, S.; Geiger, W. E. *Inorg. Chem.* **2009**, *48*, 2156–2165. (b) Todd, M. D.; Dong, Y.; Hupp, J. T. *Inorg. Chem.* **1991**, *30*, 4688. (c) LeSuer, R. J.; Buttolph, C.; Geiger, W. E. *Anal. Chem.* **2004**, *76*, 6395. (d) Trupia, S.; Nafady, A.; Geiger, W. E. *Inorg. Chem.* **2003**, *42*, 5480–5482.
- 14 Amatore, C.; Gareil, M.; Saveant, J. M. *J. Electroanal. Chem.* **1983**, *147*, 1–38.
- 15 Kuwana, T.; Bublitz, D. E.; Hoh, G. *J. Am. Chem. Soc.* **1960**, *82*, 5811–5817.
- 16 Kukhareenko, S. V.; Strelets, V. V.; Kudinov, A. R.; Kreidlin, A. Z.; Peterleitner, M. G.; Denisovich, L. I.; Rybinskaya, M. I. *J. Organomet. Chem.* **1996**, *519*, 1–5.
- 17 Hargrove, D. C.; Templeton, D. H. *Acta Crystallogr.* **1959**, *12*, 28.
- 18 Messina, P.; Labbé, E.; Buriez, O.; Hillard, E. A.; Vessières, A.; Hamels, D.; Top, S.; Jaouen, G.; Frapart, Y. M.; Mansuy, D.; Amatore, C. *Chem. Eur. J.* **2012**, *18*, 6581.
- 19 Görmen, M.; Pigeon, P.; Hillard, E. A.; Vessières, A.; Huché, M.; Richard, M.-A.; McGlinchey, M. J.; Top, S.; Jaouen, G. *Organometallics* **2012**, *31*, 5856–5866.